Korean Chem. Eng. Res., 62(4), 296-311 (2024)
https://doi.org/10.9713/kcer.2024.62.4.296
PISSN 0304-128X, EISSN 2233-9558

총 설

A Review of Experimental and CFD Techniques to Characterize Macromixing via the Intensity of Segregation in a Rotating Bar Reactor

Abdelgadir Bashir Banaga*,,***,† and Zeinab A. M. Khalel*,****

*Research Center of Sudan for High Gravity Engineering and Technology, Khartoum, Sudan
**Sudan University of Science and Technology, P.O. Box 72, Khartoum 11111, Sudan
***Research Center of the Ministry of Education for High Gravity Engineering and Technology, Beijing University of Chemical Technology, Beijing 100029, PR China
(Received 22 July 2024; Received in revised from 24 September 2024; Accepted 24 September 2024)

Abstract – Several experimental and Computational Fluid Dynamics (CFD) methods have been developed to analyze and describe macromixing processes in a rotating bar reactor (RBR). This review provides an overview of the measurement methods of macromixing and delivers an assessment based on the concentration field. The concentrations are directly used to define the intensity of segregation (I_s), and can reflect macromixing in a rotating bar reactor. Additionally, shows the investigations of the techniques available for portraying the intensity of segregation. This research is organized into three primary sections. The initial two sections focus on the overarching trends associated with the implementation of Conductivity, Planar Laser-Induced Fluorescence, and Electrical Resistance Tomography methods in RBR. An examination of the procedural steps, materials utilized, and the associated calculations was conducted. The final section addresses the simulation model of Computational Fluid Dynamics (CFD), detailing the necessary parameters, including the equations employed, boundary conditions, and the calculation procedures for determining the intensity of segregation. Subsequently, the study elucidates the feasibility of employing CFD as a precise technique for evaluating macromixing. The experimental techniques available were reviewed and compared in terms of their advantages, disadvantages, characterization capabilities, and scope of application.

Key words: Intensity of segregation, Conductivity, PLIF, ERT, CFD

1. Introduction

Process technology operations require enhanced mixing performance leading to better overall reaction rates, yields, and selectivity to the desired products. Thus, multiple investigations on reactor configurations were conducted to intensify the mixing [1]. Mixing quality in various reactors has been studied, including the rotating packed bed reactor (RPB), Taylor Couette (TC) reactor, microchannel reactor, rotating bar reactor (RBR), and helical tube reactor (HTR). One typical example is the rotating bar reactor, which can continuously mix different streams between two concentric cylinders. A rotating bar reactor consists of the inner rotating cylinder and the outer static cylinder. The primary distinction is that the rotating bar reactor modify the feeding inlet. Out of all the rotating reactors, the rotating bar reactor has garnered the most level of interest, it has successfully applied low-shear mixing, biological reactions, particle classification, liquid-liquid extraction, catalytic photochemical reactions, emulsion polymerization, wastewater treatment, etc [2]. Several authors have emphasized the significance of enhancing the current processes of RBR, namely by improving mass transfer and mixing efficiency [3- 5]. Different flow patterns may arise within the annular space of an RBR, leading to distinct flow characteristics and configurations. The blending conditions within an RBR can be adjusted almost autonomously from the axial flow, through changes in the rotational velocity of the cylinders and the reactor's geometry [5].

The performance of most industrial liquid-liquid processing is affected by the mixing of miscible fluids and mass transfer. Mixing is described as the decrease of non-homogeneity to obtain the requested process. Non-homogeneity is influenced by concentration, condition, or heat. The main factors to recognize in each mixing process are the time accessible to achieve the required mixing quality and the scale of homogeneity [1,6]. Particularly, mixing quality is a fundamental factor in deciding reactor performance [2,7], especially for fast and complex chemical reactions [3,7]. It plays a significant part in improving the quality of the final products [4,8]. Moreover, mixing in chemical reactors is a considerable unit activity, and the design and improvement of the all-around reactor are of huge viable significance in enhancing mixing [9,10]. It is accepted to partition the mixing into a cascade of macromixing, mesomixing, and micromixing [11,12]. Macromixing depicts the initial stage in the contacting of two liquids process, it happens on the gross scale of the whole mixing vessel [13]. This scale is defined as a change that occurs in mixture concentration at a reactor scale. It has a significant vicarious role in the reaction where macromixing decides the climate for mesomixing and micromixing [14,15]. Mesomixing is mixing at the coarse scale [16] and happens

† To whom correspondence should be addressed.
E-mail: asad.85@hotmail.com

quickly after the feed stream is introduced into the reactor [13,17-20]. Baldyga proposed the Batchelor scale as a metric for quantifying micromixing [21]. It alludes to the blending of specific molecules and cells for liquid, and it normally happens for the regular concentration [21,23].

Studies on measurement techniques of macromixing in the RBR are limited. Consequently, this review will present the most common techniques used. Measurement levels of macromixing are divided into two divisions, mixing level and mixing time. Two different indices to quantify mixing are the intensity of segregation and the segregation index [24]. Particularly, the segregation intensity depends on the concentration field [25]. Danckwerts introduced the scale and intensity of segregation (I_s) in 1952 to estimate mixing quality [26]. Generally, the scale of segregation represents the expansion of fluid components of steady concentration, it is a measurement of the mixing quality of the fluid elements [27]. The level of segregation can be assessed by analysing the variation in composition at individual points compared to the overall composition of the mixture, with I_s serving as a statistical measure of mixing quality [28,29]. However, I_s value can be well used to describe the macromixing state [30].

Four different techniques to quantify the intensity of segregation are commonly used, including the conductivity method [5], Planar Laser-Induced Fluorescence (PLIF), Electrical Resistance Tomography (ERT) [31], and Computational Fluid Dynamics (CFD) [32]. These methods are principally used for investigating concentration fields, which are required for evaluating the intensity of segregation. The first technique is conductivity, which has been applied to compute the concentration distribution in the axial direction of RBR. The Danckwerts principle was applied successfully to the mathematical part to complete the computation of I_s. This method is done experimentally by adding a sodium chloride solution and mixing it with deionized water into the rotating bar reactor [5]. The second technique, PLIF is used to track liquid flows in different mixing channels [33,34], and measure the concentration field inside the reactor [24]. The third method can distinguish changes in conductivity/resistivity, it is generally applied for hydrodynamic examinations of the blending elements of mixable liquors [35]. The most important element in the ERT, which employs electrodes inside set up at the vessel dividers, is in touch with the interaction substance [36]. In order to save time and provide quick methods for measuring macromixing, CFD is a significant breakthrough in understanding mixing processes in reactors. Finally, Computational fluid dynamics has become a basic numerical method in the analysis of fluid dynamics. To date, CFD can be successfully applied to the design and analysis of parts of devices similar to the mixers [37]. Consequently, CFD is considered an effective technique for assessing the intensity of segregation [15]. Figure 1 reconstructed macromixing characterization techniques examples from conductivity, PLIF, ERT, and CFD.

Evaluating the effectiveness of mixing is crucial for the advancement of reactor design. Given the significance and complexity of mixing

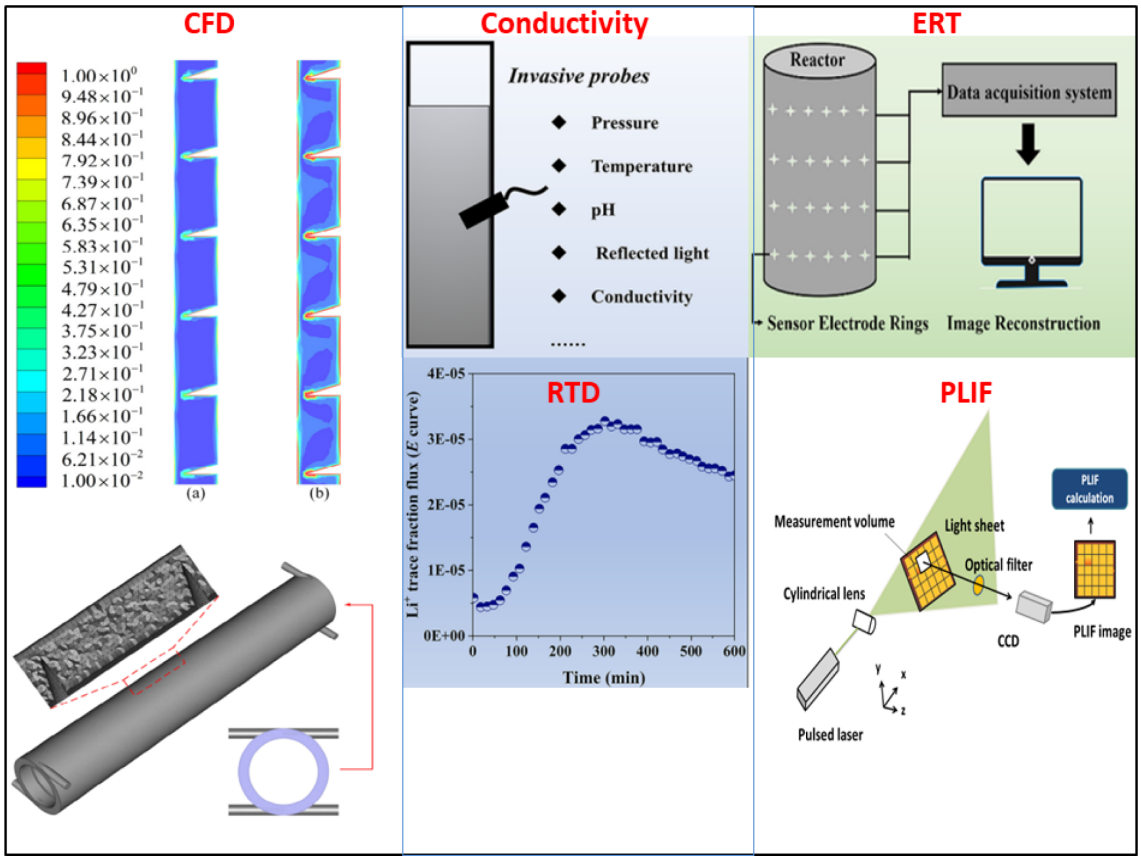

Fig. 1. Experimental techniques for characterizing macromixing performance.

in the reaction process, several techniques have been devised to investigate macromixing in reactors, mostly employing physical methods and CFD [38]. Over the years, various methods have been invented to characterize macromixing for liquid-liquid systems. This review has presented an analysis of the main important methods that were used to evaluate macromixing via the intensity of segregation in a rotating bar reactor, and common trends for the most essential operational and design factors of RBR will be deduced. Since there are not enough publications that describe a complete system assessment of macromixing in RBR, they have been the focus of this review and analysis. Our work aims to give details of conductivity, PLIF, ERT, and CFD techniques that have been developed to characterize the macromixing in RBR. A review of the significant factors was clarified, for example, materials utilized, types of equipment, dyes used, experiment steps, and equations for I_s assessment. A Comparison of the Conductivity, PLIF, and ERT methods was organized. This comparison aims to compare the advantages and limitations of each of the described techniques and offer some direction as to which technique may work for a particular need or application.

2. RBR Technology

The RBR shows great potential for enhancing process efficiency. The RBR is furnished with an improved feeding mechanism that integrates radial and tangential feeding modes. The reactor's efficiency is affected by the type of feeding inlet. The distribution of axial velocity was more uniform when the reactor functioned with the tangential inlet compared to the other inlets. The RBR with tangential feeding mode exhibited exceptional micromixing performance, achieving a micromixing time of approximately 10^{-5} s [2-4]. In addition, the RBR provided the benefits of a rich cascade of various flow states that created a variety of hydrodynamic circumstances, including both laminar and turbulent conditions [39]. The flow regime can be customized to meet the specific needs of mixing and dispersing by controlling excessive shear forces and extreme flow segregation, resulting in a plug-flow feature [40]. In these conditions, a liquid flow outside of the axis, moving from the bottom to the top, counterbalances the flow patterns. Therefore, as the axial flow increases, the vortices expand out in the same direction as the flow. Significantly, the turbulence RBR flow combines the advantages of intense mixing with small axial dispersion [1,41]. The rotating bar reactor is process intensification equipment that offers several advantages. It exhibits excellent micromixing performance, and the rapid mixing of fluids in the reactor is facilitated by the high-speed rotation of the inner axis. The rotating bar reactor exhibits much higher mass transfer and mixing efficiency as compared to rotating reactors. Hence, the duration that the fluid remains in the RBR can be regulated, making it suited for quick, medium, and slow reactions [2].

2-1. Basic structure of the rotating bar reactor

Figure 2(A) demonstrates the design of the RBR, which includes both inner and outer cylinders. The outer cylinder is equipped with fixed radial and tangential feeding inlets. The geometric dimensions are presented in Table 1. Figures 2(B), (C) demonstrate tangential and radial feeding modes, respectively. The feeding method is referred to as tangential feeding mode when solution A (the primary solution) is introduced through the tangential tube at a greater flow rate than solution B. The feeding method is referred to as the radial feeding mode when solution A (the main solution) is introduced vertically into the outer cylinder through the input tube at a higher flow rate than solution B.

The RBR and TC reactor differ in two aspects: i) The RBR is equipped with an enhanced feeding system that includes two or more entry points, enabling the introduction of several reagents into the RBR with an appropriate method of premixing. ii) Typically, the

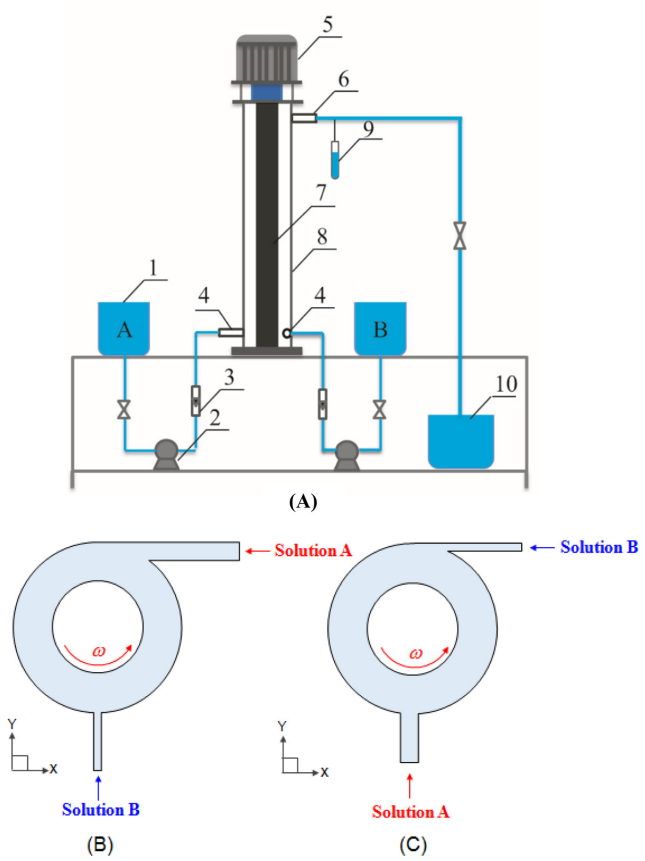

Fig. 2. Schematic diagram of the (a) experimental setup (1-tank A, 2-pump, 3-flow meter, 4-inlet, 5-motor, 6-outlet, 7-inner rotating cylinder, 8-outer cylinder, 9-sampling point, 10-drain tank), (b) tangential feeding mode, and (c) radial feeding mode (Solution A: the main solution).

Table 1. Rotating bar reactor dimensions

Items	Values
Outer cylinder radius (R_o)	15 mm
Inner cylinder radius (R_i)	10 mm
Gap width (d)	5 mm
Length (L)	445 mm
Aspect ratio ($\Gamma = L/d$)	89

RBR operates at a higher rotational speed in comparison to the TC reactor. The rotating bar reactor has garnered significant interest recently due to its excellent mixing capabilities [2]. Gao et al. employed RBR to improve the efficiency of ozone-water mass transfer by optimizing its internal configurations. The finding showed that RBR has the ability to achieve an equivalent rate of decolorization with a reduced amount of ozone dosage. The RBR has shown significant potential for improving liquid film control [3]. RBR provided an annular zone as the location for mixing and mass transfer. The rotation of the inner bar greatly enhanced the disturbance intensity of the fluid in the annular zone of the RBR, thus impacting the efficiencies of mixing and mass transfer [4]. The wastewater treatment has been usefully applied in RBR [42].

3. Macromixing

Macromixing is the term used to describe mixing at the reactor scale. The convection of the fluid particles inside the flow domain specifies the concentrations in the environment. Macromixing can be evaluated using measurement methods, including residence time distribution and segregation scale. The residence time distribution (RTD) method is typically used to describe macromixing as an indicator of velocity field uniformity. The RTD is straightforwardly associated with the overall movement of the flow since it addresses the time the liquid particles consume to relocate from the device inlet to the outlet. This macro-scale movement, brought about by the mean flow acceleration, drives the liquid particles among high and low-momentum locales in the reactor volume, deciding the huge scope of convective transfer named macromixing [15]. However, because macromixing is strongly determined by the flow behavior inside the reactors or vessels, converting the conditions for micromixing may be particularly affected by macromixing [43]. Therefore, based on the concentration variance, the intensity of segregation is considered an accurate scale to evaluate the macromixing. From the previous research, the conclusion reflected that the methods used focus on calculating the time needed for completed mixing, therefore this review will discuss methods for measuring macromixing through concentration differences in the RBR scale.

The process of macromixing involves the homogeneity of concentrations at the reactor scale [44,45]. It determines the condition concentrations for smaller scaling processes and conveys fluids through environments where turbulent properties vary [46]. From this vantage point, the intensity of segregation can be used to measure macromixing. The reason for the relationship between macromixing and the intensity of segregation is the level of homogeneity in concentration. In the literature, the coefficient of variation (C_oV) acts as a measurement scale of macromixing [47], and it has been found that the intensity of segregation is directly related to it [48]. The quantitative appearance of the macromixing in the dispersed phase is determined by the spatial variance of the tracer concentration [49].

4. Measurement Methods of the Intensity of Segregation

The intensity of segregation is quantified by employing either the concentration variance or the coefficient of variation. Distributive mixing is comparable to the intensity of segregation and pertains to the dispersion of any additive across the entire volume [50]. The segregation intensity was employed as a quantitative scale to measure macromixing, which reflected the degree of variation in concentrations throughout the whole reactor [30]. Indeed, the definition of macromixing reflects the changes in mixture concentration on a reactor scale. Different techniques have been employed to assess the distribution of concentration within an RBR during the process of liquid-liquid mixing. The accurate methods employed to evaluate I_s encompass the conductivity method [5], Planar Laser-Induced Fluorescence [51,52], Electrical Resistance Tomography [31], and CFD simulation [53].

4-1. Conductivity method

The conductivity method is an invasive technique that can accurately measure the concentration at different levels along the RBR. The method of conductivity is also employed to determine the average residence time distribution to characterize macromixing [5,54]. This method enables the estimation of concentration distributions with great precision. Conductivity serves as an approximation of a solution's capacity to conduct an electric current. It is influenced by factors such as temperature, concentration, mobility, and the valence state of ionized species in a liquid. Solutions of inorganic compounds exhibit appropriate conductivity, but solutions of organic mixtures that no longer dissociate in water have weak conductivity. Therefore, this approach is exclusively applicable to solutions that possess high conductivity. The conductivity strategy can be easily implemented provided that the necessary materials are available. This article presents a way of assessing the intensity of segregation based on the conductivity method. The approach has numerous benefits, such as the capacity to operate under various conditions, precision, and the capability to gather data within the reactor. One of its key benefits is the utilization of a limited number of devices, which is regarded as the most economical option [5]. The primary aim of this set of experiments is to examine the efficiency of mixing along the RBR. Banaga et al. conducted a research study on the segregation intensity at various levels along the axial direction of RBR. They used the conductivity approach to directly measure the concentration field. The study examined the impact of rotational speed, flow rate, reactor height, and NaCl concentration on the I_s.

4-1-1. Experimental section

Figure 3 depicts a complete RBR setup, showcasing all its components. A sampling system was designed to take 24 samples at a time. The sampling locations were positioned at four different levels along the RBR. Typically, the entrance of the rotating bar reactor was regarded

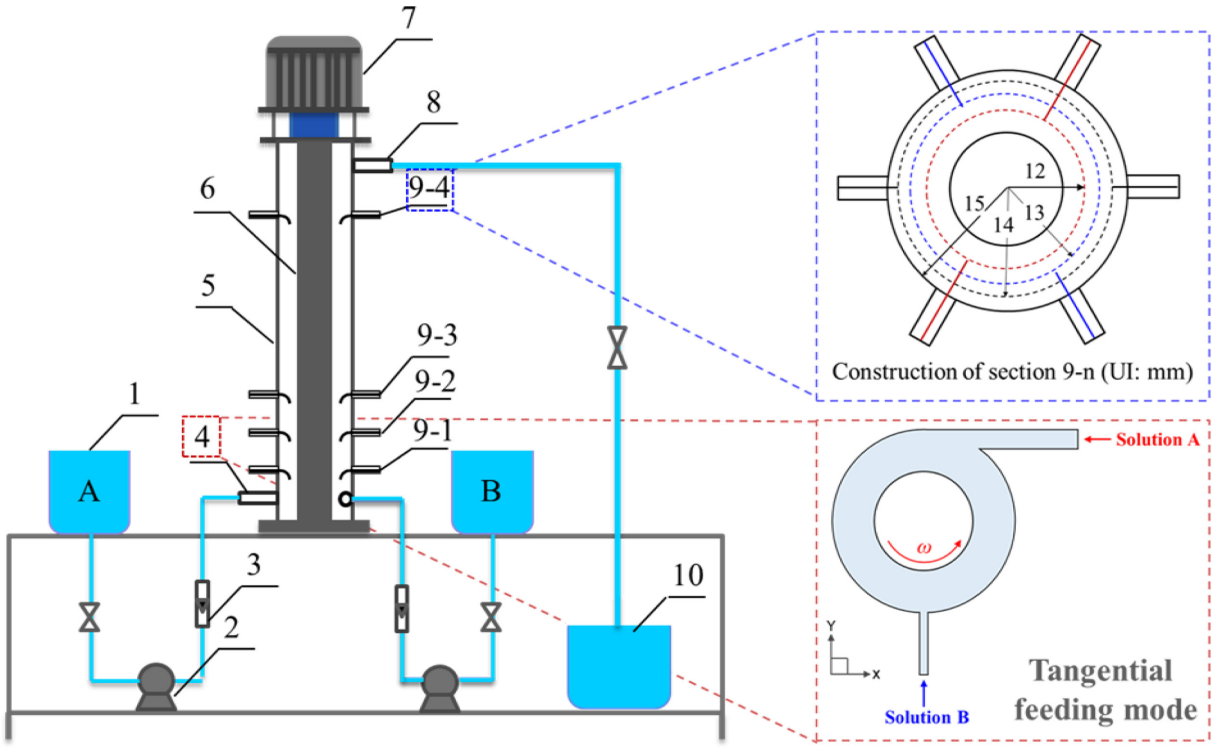

Fig. 3. Schematic diagram of the experimental setup: 1-tank, 2-pump, 3-flow meter, 4-inlet section, 5-outer cylinder, 6-inner rotating cylinder, 7-motor, 8-outlet, 9-1 sampling level 1 (bottom section), 9-2 sampling level 2, 9-3 sampling level 3, 9-4 sampling level 4 (top section), 10-drain tank.

as a fundamental plane. The second section was the top section, with a sampling plane at a distance of 330 mm from the bottom of the reactor and 62 mm from the outlet. Each plane comprised of six sampling locations located within the same cross-sectional region. The samples were drawn by the small tubes at varying distances from the outer cylinder of the reactor, specifically at 1, 2, and 3 mm away from the wall. The design of the sampling system is clarified in Figure 3 [5].

A conductivity-based technique was developed and successfully employed to assess macromixing by analyzing the concentrations of acquired samples. The primary determinant in conducting conductometry was the rapid response time of the probes [54]. This method used a strong electrolyte, and NaCl solution served as a tracer. Solutions B and A were prepared in vessels from 100 g/L NaCl solution and deionized water, respectively. Two peristaltic pumps were used to feed the solutions into the RBR. Solution B was injected into the reactor through the radial tube at a flow rate of V_B, while solution A introduced into RBR through the tangential tube at a flow rate of V_A. In the majority of experiments, the ratio between V_A and V_B (V_A: V_B) remained constant at 10:1.

The solutions flowed up the RBR to a drain vessel via the outlet. A motor regulated the rotational speed of the inner cylinder, enhancing the macromixing. Five minutes after the experiment commenced, samples were collected from four distinct levels, with six samples taken from each level at the same time. The conductivity of the sample was determined using a conductivity meter. The calibration equation, which was based on the linear relationship between the concentrations

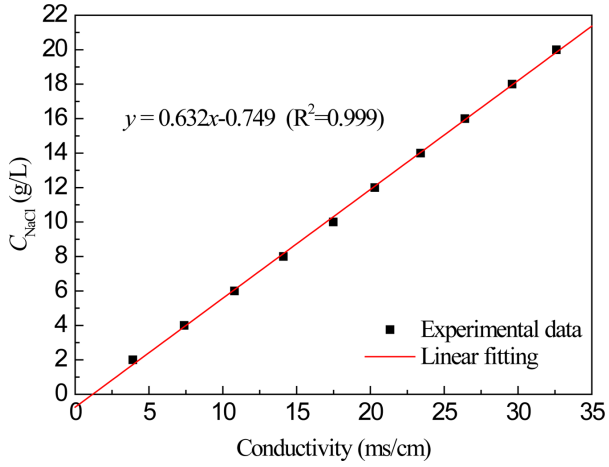

Fig. 4. Calibration equation and curve based on the linear relationship between concentrations of the NaCl solution and conductivity.

of the NaCl solution and conductivity, was used to convert conductivity values into concentration data. This conversion process is illustrated in Figure 4. The macromixing was indicated by the concentration domain within the RBR. Local segregation intensity can be measured at various locations within the reactor. Table 2 shows the experimental conditions [5].

4-1-2. Evaluation of macromixing

In this case, macromixing was described by the I_s which depends

Table 2. Specifications of the experimental conditions

Items	Values
Rotational speed, N	0–700 r/min
Flow rate of solution A, V_A	30–110 L/h
Flow rate of solution B, V_B	5–10 L/h
Sodium chloride concentration, C_{NaCl}	10–300 g/L
RBR length, Z	62–330 mm

on the concentration of species A and B, and was determined as:

$$I_s = \frac{\sigma_0^2}{\sigma_m^2} \tag{1}$$

$$\sigma_0 = \sqrt{\frac{\sum \left(x_i - \bar{x}_{av}\right)^2}{n}} \tag{2}$$

$$\sigma_m = \sqrt{\bar{x}_{av}\left(1 - \bar{x}_{av}\right)} \tag{3}$$

The standard deviation was denoted as s_0, which signified the root-mean-square average deviation of contents within the cross-section. The mass fraction of a species at a specific sampling point i denoted as x_i, was determined by calculating the conductivity values. The total number of sampling points in a selected sampling section was represented by n. s_m was the initial value of the concentration variance, while $\bar{x}_{av}$ was the average mass fraction. According to Equation 1, the value of I_s was determined within the range of 0-1. A value of zero indicated the highest level of mixing performance, whereas a value of 1.0 represented the lowest level of mixing performance [15,53]. The mean concentration of NaCl (C_{av}) was estimated corresponding to the concentrations and flow rates of solutions A and B, as indicated in the following Equation:

$$C_{av} = \frac{C_{Nacl} V_B}{V_A + V_B} \tag{4}$$

The volumetric flow rates of solutions A and B were denoted as V_A and V_B, respectively [5].

The findings showed that the inhomogeneity of the concentrations appeared at the bottom of the RBR, and the homogeneity was generated at the top section. The intensity of segregation gradually decreased along the RBR from 10^{-5} to 10^{-7}. On the other hand, the increases in the rotation speed, the flow rate of solution A, and the decline in the NaCl concentration and flow rate of solution B resulted in a decrease in I_s. Increasing the flow rate led to a reduction in segregation intensity compared to the other cases, signifying an improved mixing efficiency [5].

4-2. Planar Laser-Induced Fluorescence

The PLIF offers a non-intrusive approach to quantitatively measure concentration distribution within an illuminated flow field, providing high temporal and spatial resolutions. This system characterizes the mixing impacts by examining concentration dispersion. The mixing attributes downstream of the spacer network are quantitatively and qualitatively examined based on the examination of concentration dissemination [55,56]. Several studies, mostly using the PLIF method to evaluate the concentration field have been conducted [57,58]. Mahsa Taghaviab et al. and K. Kling et al. also used PLIF to measure the advancement of mixing within the reactor [24,34]. Hence, the PLIF method was employed to investigate the blending procedure of the T-jets mixer. Tap water served as the operational fluid, while Rhodamine 6G acted as the fluorescent marker. A persistent laser was utilized to stimulate the fluorescence, and the CCD camera captured the emitted fluorescence light. The distribution of fluorescence intensity on the measurement plane can be transformed into the distribution of tracer concentration. Approximately 500 images were captured in each experimental run, which corresponds to a total sampling time of 5~10 seconds [59].

In recent years, some researchers used the PLIF technique with different experimental setups. Eltayeb et al. [60] applied the PLIF technique in a down-comer reactor, to examine the coolant blending technique. In which the PLIF method was applied to examine the boron mixing phenomena. The typical concentration at two points inside the reactor was discovered by PLIF measurement data. Using the advantages of this technique, the effects of different slug densities on mixing behavior in the vessel downcomer were analyzed, in addition to the possibility of calculating the mass fraction at the given location. The experiment setup consisted of a hemispherical reaction tank, power supply, high-speed camera, double laser sources, four vessels, pumps, an electromagnetic flow gauge, temperature indicator, junction pipes, valves, a pressure gauge, and the data acquisition system. Eltayeb et al. [60] agreed with Taghavi et al. [34] that the experiments took place in a stirred tank equipped with baffles. The setup was done without using mirrors, and injected one kind of dye, also, the laser sheet with 532 nm wavelength was lighted the whole center cross-section of the mixing vessel. To avoid possible laser radiation reflections, they painted the impellers a matte black color. The characteristics of the laser used should be taken into account, such as laser type, energy per pulse, pulse duration, and emission wavelength. In addition, a high-pass visual filter was located forward of the camera lens to gain the fluorescence light while refusing the laser illumination, and to eliminate the interference effect of lighting and emission. Many parameters can be taken into consideration, for instance, the flow conditions, and pressure adopted. The field of the mixing zone, the size of the pixel, and the total volume should also be determined.

PLIF is a measurement technique dependent on fluorescence released from the species agitated by planar radiation light. Ultimately, a sheet of laser light is carried over a flow domain. Then easily the subsistence and concentration of a species can be specified out of its features fluorescence whilst agitated by a laser source. The strategy is generally utilized to quantify integral-domain concentration maps in liquid flows. Customarily, a well-set-up visual absorption transition of the species to be analyzed is selected and corresponds to the laser excitation wavelength. In this practice, the atom is moved to an agitated condition via a laser light sheet whose wavelength is harmonized to agitate a particular transition. The fluorescence is caught on a CCD (Charged

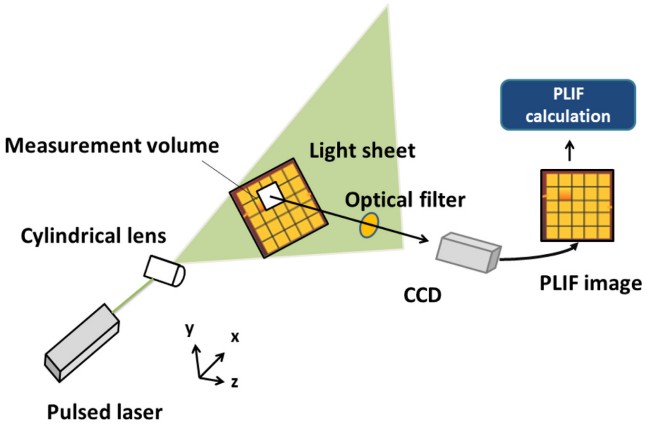

Fig. 5. Optical setup for the Planar Laser-Induced Fluorescence.

Coupled Device) imaging sensor and enables the obtaining of spatial data on the concentration and the effectiveness of the species [61,62].

4-2-1. Experimental section

The concentration domain of twin fluorescent pigments was estimated in the mixing vessel using the PLIF. The pulsed laser with wavelength λ = 495 nm was spent as a light source. The laser radiation was expanded using a strategy of ball-shaped and cylindrical lenses. At the point when a fluorescent color was illuminated in a vessel of the different light sheets it enlightened a region in the blending vessel. The CCD camera was set vertically to distinguish the emitted light. The visual setup is illustrated in Figure 4 [63].

The procedure involved injecting a blend of an inactive and a responsive fluorescent dye into the reactor. The inactive dye acted as a tracer for the macromixing process. The responsive dye altered its fluorescent characteristics as it underwent a rapid chemical reaction with the reactor contents, thereby indicating the micromixing indirectly. The intensity of the illumination was evaluated at specified gray values. To differentiate the fluorescent light of dyes, two optical filters were used. The dual-picture optics were utilized to discover the same presentation window two times simultaneously. It included two slots that were supplied with double filters, besides a group of convertible and stationary mirrors. The mirrors reflected the fluorescent illumination onto the illumination-sensitive camera wafer; hence the same exhibit window was shown alongside, the camera wafer with one-half each ideally the fluorescent light sent out by the fluorescent dyes. The computer has been used to control the exhibition of the camera along with the pulse of the laser. Before starting the experiments, some parameters should be determined, such as the highest gauging frequency the resolution of the camera, and maximum flow rate amounts. Assessments were conducted in a plane-bottomed, transparent vessel with a specific diameter. It was located inside a box full of water to reduce reflections and deformation at the cylindrical walls. The reaction tank was full out to a specific height, and the blade numbers of the Rushton turbine were located inside the reaction tank, to obtain a lower Reynolds number [24].

The characteristics of the laser used should be taken into account, such as laser type (a pulsed Nd: YAG laser), energy per pulse, pulse duration, and emission wavelength. Furthermore, a high-pass optical filter was positioned in front of the camera lens to capture the fluorescence light while blocking out the laser light, and to minimize any potential interference from ambient lighting and emission. Many parameters can be taken into consideration, for instance, the flow conditions (velocity), and pressure adopted. Furthermore, the dimensions of the mixing zone (mm*mm), the size of the pixel, and the total volume should be determined [64].

On the other hand, many researchers have utilized the benefits of using both methods, Particle Image Velocimetry (PIV) and PLIF simultaneously. A couple of PIV and PLIF measurements were employed to characterize the flow and mixing in a Taylor Couette reactor. The examination of passive tracer measurements' concentration was employed to explore the efficiency of mixing across various flow patterns. The PLIF method effectively captured concentration maps across a full plane without the need for a physical probe. This was concerning the research on fluid flow and mixing, utilizing planar laser-induced fluorescence and particle image velocimetry techniques. The combination of PLIF and PIV techniques has provided a comprehensive understanding both qualitatively and quantitatively [65]. Additionally, by integrating the PLIF technique with the PIV

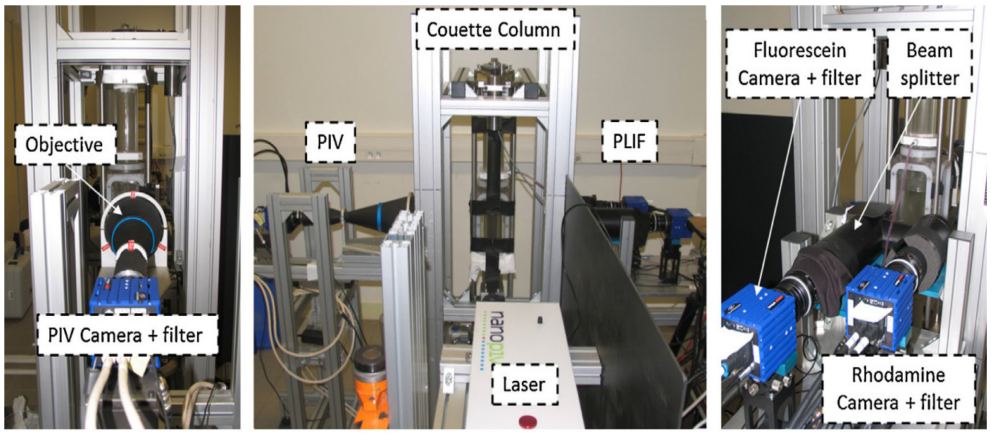

Fig. 6. Experimental devices for the coupled PIV/PLIF measurements.

technique, valuable information regarding velocity and temperature in the flow field can be obtained [66]. The setup of experimental devices for the coupled PIV/PLIF measurements is presented in Figure 6 [67].

4-2-2. Evaluation of macromixing

The PLIF was used as an accurate technique to determine the intensity of segregation. According to Danckwerts' 1952 proposal on segregation intensity, the macromixing quality can be estimated. Equation (1) was used to calculate the intensity of segregation as an indicator of macromixing. The mixing index was based on the concentration standard deviation and the maximum mean concentration [34,67].

4-2-3. Dye types used in the PLIF technique

The PLIF method can use different kinds of dyes, and the popular dyes are fluorescein together with Rhodamine dyes (Rhodamine 6G, Rhodamine B, Rhodamine WT). All of the dyes should be water-dissolvable. Fluorescein is the most commonly utilized dye. The fluorescein peak absorption is close to 490 nm, peak emission near 510 nm, and has moderately low affectability to temperature variation. Nonetheless, the absorption spectrum of fluorescein substantially relies on pH, with absorption turning into the power of hydrogen being less than four [68,69]. This pH affectability may be abused for blending examinations. The term fluorescein is thought to be prone to photobleaching [70,71] however, this hassle has been proven to be minimal for standard PLIF implementations [70]. Rhodamine 6G has a peak absorption near 525 nm and a peak emission near 560 nm. In addition, it is extremely resistant to photobleaching [71,72]. Temperature and pH reliance information for this pigment are scant.

Rhodamine B exhibits a prominent peak near 555 nm, although its absorption spectrum is wide enough to enable excitation at 514.5 nm. The fluorescence of Rhodamine B is sensitive to variations in temperature [73-75], however rather insensitive to adjustments in pH. The sensitivity to temperature changes can be leveraged to utilize PLIF for temperature measurements. Rhodamine B may have intense and chronic well-being impacts in the event of skin or eye connection, inward breath, or ingestion, and is viewed as by a wide margin the most harmful of the xanthene pigments [76]. Rhodamine WT has comparable spectral traits to Rhodamine B and has been utilized in some PLIF experiments [64], and is probably a more secure opportunity for Rhodamine B for lots of experiments.

Explaining the use of dyes in the PLIF method is useful by taking Rhodamine B as an example. Rhodamine B can be utilized as the fluorescent tracer with a certain concentration; a tracer solution should be prepared and pumped into one liquid stream. The experiments were carried out by introducing two solutions into the mixing vessel, the first one was pure water, and the second one was water with Rhodamine B. A laser sheet was used to illuminate the mixing region for the two liquids. The agitated fluorescence intensity as a result of the existence of Rhodamine B was taken via a CCD camera and treated to become a tracer concentration of the mixture. The post-treatment of the pictures was performed using suitable software [64].

4-3. The Electrical Resistance Tomography

ERT is one of the accurate methods for the dynamic assessment of mixture homogeneity [48,77]. The fundamental rule of ERT is that in order to get data on the inward composition or electrical properties of the mixture into a cross-segment of the specified equipment, combining multiple estimations from points inside the device is required. Electrical resistance tomography can expand scaling time for developing the concentration domain. The object of ERT is to determine the resistance distribution, while the distribution of the resistance in a cross-section can be obtained by inserting current on the domain and calculating voltages. Another meaning is that Electrical resistance tomography can discover local variations in conductivity, this method normally applies to hydrodynamic investigations of the unstable mixing, and dynamics of miscible liquors if the liquids to be mixed vary in conductivities [78]. ERT is a non-invasive method that has been applied appreciably to evaluate blending properties under diverse processes [79], and different equipment, such as mixing vessels [80,81], rotating separators [82], bubble columns [83], packed columns[84], hydro-cyclone [85], circulating fluidized beds [86], pipes and reactors [78]. Within the specified area of voltage estimations on the vessel periphery, ERT gauges the distribution of electrical conductivity [87].

ERT is an appealing technique for opaque systems, making it a perfect fit for research purposes and industrial applications [88], as illustrated by publications on industrial tomography [78]. By using ERT, the distribution of the disseminated phase concentration may be decided in either two-phase system as long as the conductivities of the continual and also scattered phases are distinct enough, identically to conductivity probes [89]. In general sight, the ERT framework demands a sensor system, a Data Acquisition System (DAS), and a computer with control and information processing programming. The sensor comprises numerous electrodes organized equally spatially about the interested zone in the form of one or more electrode rings. The most well-known arrangement was a roundabout vessel with 16 electrodes [78]. The sensors are normally made from gold, platinum, stainless steel, brass, or silver and should have qualities like minimal expense, simplicity of establishment, resistance in addition to excellent conductivity [87].

The Data Acquisition System is the unit that infuses current and gathers the quantitative data portraying the conductivity dispersion inside the determined vessel for mixing. It comprised of signal sources, a system of electrode demodulators, electronic voltmeters, signal demodulators, as well as a control unit. The DAS is associated with the electrodes and the computer including the picture reconstruction algorithms. Mutual current is infused from the DAS to the electrodes utilizing a couple of neighboring electrodes and the ensuing voltage is measured via all different neighboring electrodes [78].

Concerning the particular examination of liquid mixing, several past works have been published on the examination of various mixing

vessels. Yenjaichon et al. [90] assessed the quality of blending a pulp suspension and chlorine dioxide in a static blender and applied electrical resistance tomography. The homogeneity was measured by a mixing index dependent on the coefficient of variation of the singular conductivity values in each picture pixel. ERT measures the dispersion of electrical conductivity in the area of interest from voltage estimations. In the case of the experiment carried out, a 610 mm ID Polytetrafluoroethylene (PTFE) gasket was embedded within the flanges after the fixed blender. The evaluation level consists of circular titanium electrodes (sensors). Every electrode was strung into the PTFE gasket to be flush with the inward mass of the plane. To connect the cables that provide input and output electrical signals, a screw was inserted at the edges of each electrode. All electrodes had been associated with an ITS (Industrial Tomography Systems Ltd) Z8000 system. The ITS Z8000 method applied a steady alternating current to a couple of electrodes and estimated the voltage contrasts between the other electrodes set utilizing a contiguous pair procedure. Meanwhile, the sampling interval was once maintained at a hundred ms. A linear back-projection algorithm used to be employed for picture rebuilding in the usage of ITS Z8000 software [90].

Over the previous decade, ERT techniques were effectively applied to assess various processes. Pakzad et al. [91] carried out the ERT method to assess the cavern formed around a Scaba impeller in the blending of yield-pseudoplastic fluids. The blending overall performance of a solid-liquid system was estimated via the ERT method by Hosseini et al. [92]. They evaluated the impact of sizeable parameters on the level of homogeneity which included blade type, blade speed, blade off-bottom clearance, and particle volume. Tahvildarian et al. used ERT the method to examine solid-liquid blending in a slurry reactor [31]. Furthermore, the study delved into analyzing the effects of identical variables previously examined by Hosseini et al. [92], while also considering the impact of particle volume and solids concentration on the uniformity of particles in the suspension reactor. Using ERT, Carletti et al. estimated a solid-liquid system by evaluating the locative concentration of the dispersed phase. According to their findings, it was concluded that the uniformity decreased when the solid loading was increased [93]. Mirshekari et al. carried out the ERT method to examine the mixing execution of liquid-liquid scattering systems in expressions of the mixing scale. The operating fluids had faucet water as the continuous phase, and three various sorts of oils as the dispersed phase. The impact of the conditions and impeller parameters on the mixing scale was studied during the layout of the experiment and reaction surface manner [94].

4-3-1. Experimental section

The local distribution of the diesel fuel in the water was assessed on four horizontal areas of the stirred tank from the conductivity of the mixture estimated with the ITS 2000 ERT instrumentation. The electrodes were set on the inside tank wall and then associated with the Data Acquisition System. The estimations depended on the circuitous adjacent methodology, in which electric flow was infused from a nearby terminal pair at a time and the voltage contrast was estimated from the excess sets of anodes. Concerning the reproductive strategy for getting the conductivity maps from the electric possible estimations, the linearized adjusted sensation back-projection algorithm was chosen, as executed in the ITS System. The conductivity on each plane was obtained; the estimations have appeared regarding dimensionless conductivity that was registered as the proportion between the conductivity, estimated in the fluid combination and reference conductivity. The transitions between regimes have been distinguished from the conductivity estimations on the four planes. For identifying the progress between the two regimes, the mixing index was determined by Equation (1) [95]. The ascertaining of the mixing index was done depending on the individual concentrations in each picture pixel in each picture plan. Consequently, the level of variety in the resistivity esteems in a given plane can be communicated as a standard deviation [96].

This review aims to evaluate the feasibility of utilizing the ERT system in a rotating bar reactor, building upon earlier studies. The water was introduced into the reactor by the tangential inlet, while the diesel fuel was fed through the radial inlet. According to Figure 2, the ERT system can comprise four planes that were connected. The ERT zone was equipped with a device that provided real-time cross-sectional images and data on conductivity and concentration distribution. The presence of a continuous phase allowed for the measurement of the reference voltage or current using 16 electrodes per plane. Furthermore, by incorporating the dispersed phase within the annulus, it became possible to assess the alteration in reference current. Before the beginning of each experiment, the system's current was calibrated using pure water, assuring the absence of any air pockets.

The ERT systems were equipped with data logging software named ITS P2+, which included two planes, each including 16 embedded electrodes. The electrodes can both inject and detect electric currents. The electrical contact with the fluid was established, however, it did not exert any influence on the fluid's motion. The system applied an electric current to a pair of electrodes and then measured the resulting difference in voltage between the other pairs of electrodes. The DAS injected this electric current into a pair of electrodes, and the resulting voltage was measured from the adjacent pairs of electrodes while the inner cylinder and liquid were present. The system assessed the reference current value, which was stored for further experiments. A conductivity tomogram was acquired following the calibration of the system. After the calibration process was finished, the system proceed to the second step and calculated the average concentration of the distributed feed. Typically, the introduction of the dispersed phase led to the deviation of current across these electrodes, and the software calculated the resulting change in voltage value. Subsequently, a sequence of algorithms was employed to transform this alteration in voltage into concentration and conductivity profiles [97].

4-3-2. Evaluation of macromixing

Electrical Resistance Tomography can provide conductivity distribution

along the RBR. The P2+ program employed the Maxwell correlation to transform the conductivity data into a concentration [97]. The local conductivity values obtained from ERT measurement have been used to estimate the coefficient of variation (C_oV) of the picture pixels, described as the mixing index:

$$M_m = \frac{\sigma}{y} = \frac{\sqrt{\frac{\sum_{i=1}^{n}(x_i - \bar{y})}{n-1}}}{\bar{y}} \quad (5)$$

where σ denoted the standard deviation of the conductivity, y_i was the conductivity of the local mixture, $\bar{y}$ was the average conductivity, and n was the total number of pixels in the measurement plane. The mixing index decreased as the mixing quality improved, reaching zero for perfect mixing [90]. The coefficient of variety was the proportion of the standard deviation of the concentration dissemination in the blending field (intensity of segregation), divided by the concentration that would be required for perfect blending. The standard deviation was always used to describe the macromixing [98].

5. The Comparison Between the PLIF, ERT, and Conductivity Methods

Precise methods employed to evaluate I_s include Planar Laser Induced Fluorescence [25,52] and Electrical Resistance Tomography [31]. The ERT and PLIF have a different base of evaluation. ERT dimensionless depends on the conductivity, and PLIF dimensionless depends on the grayscale. The PLIF technique was employed to study liquid flows within various mixing devices [34,35]. The PLIF approach was considerably more dependable and less sensitive to variations in the measurement location compared to the probe method. Furthermore, this method provided exceptional spatial resolution without the uncertainty of seeing in the direction of the observer's line of sight. PLIF can be combined with PIV to determine velocity and temperature data in flow fields. Nevertheless, the limited dimensions of the planar laser sheet restricted the application of PLIF to laboratory-scale reactors, which required both transparent reactors and fluids [99].

On the other hand, ERT has proven to be effective in analyzing alterations in conductivity/resistivity within an opaque system [36,78]. The comparison between ERT and PLIF results revealed that ERT can effectively identify poor mixing even within the limits of its resolution, although its accuracy diminished as perfect mixing conditions were approached. This indicated that ERT has the capability to detect inadequate mixing within its resolution boundaries and the necessary conductivity contrast, offering a quick at-line measurement option for industrial professionals. The ERT technique was applied to measure the velocity fields of shampoo in pipelines and to measure mixing of industrial pulp in static mixers. Recent applications of ERT in pipe flows demonstrated potential for in-line rheometry measurements. The application of the PLIF required both the fluid and the pipelines to be transparent; so was not implementable for opaque fluids [100]. Using the conductivity method in industrial areas required modifying the design, which allowed for taking the samples from different points inside the vessel [5].

Further, the Conductivity method suggested as an intrusive approach, can ascertain the concentration of constituents at various points along the RBR. Moreover, it was employed to analyze the distribution of mean residence time and characterize the macromixing [101,102]. The method has many advantages, including flexibility of operation conditions, accuracy, and the ability to obtain data inside the reactor. One of its most essential features was using a few devices, which was considered to be of lowest cost. This method opened the way for researchers who need help obtaining devices and materials required for PLIF and ERT methods to study the mixing performance in rotating reactors [5]. Table 3 compares the PLIF, ERT, and Conductivity methods.

Table 3. The comparison between the PLIF, ERT, and the Conductivity method [5, 34, 36, 63, 88]

Technique	Devices used	Tracer used	Advantages
PLIF	CCD camera. laser an image acquisition Imaging sensor A sheet of laser light Optical filters Mirrors Computer	Fluorescent tracer	High sensitivity Different flow field variables (concentration, density, temperature) can be obtained. Use in reacting and non-reacting flow. For transparent system
ERT	A sensor system Data Acquisition System Computer Electrodes Industrial Tomography Systems Current source	NaCl	Suitable under aerated and un-aerated conditions. For transparent and non-transparent systems.
Conductivity technique	Conductivity device (Mettler Toledo)	NaCl	High accuracy Low cost For inorganic systems. Suitable for rotating reactors For batch and continuous systems. For transparent and non-transparent systems

6. Application of CFD Simulation in RBR

Studying macromixing using CFD simulation has been taken into consideration. Experiments and CFD simulations were conducted to investigate the macromixing characteristics, which encompassed the homogenization curve and mixing time. A comprehensive comparison was made between the simulation results and experimental data, considering various operating conditions including tracer injection positions, conductivity probe locations, and rotational speeds. Moreover, the simulations provided valuable insights into the macromixing behavior in the reactor by examining the flow field, velocity distribution, and mass flux [103].

Many studies in the literature have been performed on CFD to study mixing efficiency in different reactors. The computational fluid dynamics analysis of a helical tangential porous tube-in-tube microchannel reactor (HTP-TMCR) examined three key aspects: mixing index, pressure drop, and velocity distribution. Furthermore, the study investigated the influence of four geometric parameters, namely left and right helical directions, pitch, pore size, and length of the non-porous zone, on the mixing performance of HTP-TMCR. The flow and blending properties of HTP-TMCR were computationally modeled utilizing the finite volume-oriented professional tool ANSYS Fluent 2021R1 [104].

To enhance comprehension of the mixing conditions within the Taylor Couette Reactor and Rotating Bar Reactor, the flow fields of two distinct inner cylinders were simulated utilizing the commercial CFD code, FLUENT 2020R11. The geometry in ANSYS ICEM was generated based on the configurations of the two inner cylinder types. Subsequently, the computational domain was partitioned into two regions that were linked by the predetermined interface. The velocity inlet and pressure outlet were designated as the boundary conditions, along with a no-slip wall. The discretized equations were implemented using the SIMPLE algorithm. Furthermore, to confirm the correct selection of the turbulent model, significant flow characteristics can be accurately represented [105,106].

The micromixing performance was also studied using CFD simulation. An analysis was conducted on the micromixing mechanism of the ribbed Taylor Couette reactor, with a calculation of the volume-averaged energy dissipation rate. The study investigated the impact of operating parameters and rib structural parameters on micromixing performance. The findings indicated that the presence of ribs eliminated the high shear region between the vortex pairs, leading to a concentrated micromixing region on the inner and outer cylinder wall surfaces as well as the ribbed surface region. Decreasing the rib spacing, increasing the rib width, and raising the rib height enhanced micromixing and resulted in a reduced segregation index [106].

6-1. Turbulence model

Selecting a suitable flow model is one of the most complex tasks in CFD simulation. Flow can be classified into three states: laminar, transitional, and turbulent. It is commonly acknowledged that CFD simulations of the Taylor Couette reactor function under turbulent flow conditions. The methods employed to solve the turbulent Navier-Stokes equations involve dividing the turbulence models into various computational approaches. The models employed include the Spalart-Allmaras model, the Reynolds-averaged Navier Stokes model, various Reynolds stress models, large eddy simulation, and detached-eddy simulation. The Reynolds stress model (RSM) offers a comprehensive model for solving equations related to the transport and dissipation rates of individual Reynolds stresses. It was recommended for turbulent flows characterized by intense eddies or rotations due to its high computational demands [99]. The Reynolds stress model has been shown to be highly precise when applied to cyclonic flows, making it a reliable choice for calculations in the TCR [106].

6-2. Mathematical modeling

CFD simulation is an effective method for studying the mixing performance of various reactors [43,108]. CFD analysis typically involves a set of systematic procedures, which encompass the creation of geometric models, meshing of the geometry, solving the governing equations numerically, and finally, extracting and analyzing the obtained results. FLUENT, CFX, FLOWIZ-ARD, PHOENICS, and OPEN FOAM are among the frequently utilized CFD software programs [99].

ANSYS Fluent was utilized in this study to enhance comprehension of the macromixing in the RBR. The governing equations considered in this simulation include the continuity, momentum, and species transport equations without volumetric reaction. The expressions for the continuity and momentum equations were as follows:

$$\frac{\partial \overline{U_J}}{\partial x_j} = 0 \tag{6}$$

$$\frac{\partial \overline{U_J}}{\partial t} + \frac{\partial}{\partial x_j}(\overline{U_\iota U_J}) = -\frac{1}{\rho}\frac{\partial \overline{P}}{\partial x_j} + \frac{1}{\rho}\frac{\partial \tau_{ij}}{\partial x_j} \tag{7}$$

The decomposition of U_i involved a mean part and a fluctuation U_i', while the stress tensor was expressed as:

$$\tau_{ij} = \mu\left(\frac{\partial \overline{U_\iota}}{\partial x_j} + \frac{\partial \overline{U_j}}{\partial x_i}\right) - \rho\overline{u_\iota' u_J'} \tag{8}$$

The Reynolds stress model was selected as the best model to simulate the flow in the Taylor Couette reactor, and the results showed the best agreement with the experimental data, thus, the Reynolds stress $-\rho\overline{u_\iota' u_J'}$ can be expressed as:

$$\frac{\partial(\rho\overline{u_\iota' u_J'})}{\partial t} + \frac{\partial(\rho\overline{u_\iota' u_J'})}{\partial x_k} = -\frac{\partial}{\partial x_k}[(\rho\overline{u_\iota' u_J' u_k'} + \overline{p(\delta_{kJ}u_\iota' + \delta_{\iota k}u_J')})] + \frac{\partial}{\partial x_k}(\mu\frac{\partial(\rho\overline{u_\iota' u_J'})}{\partial x_j}) \tag{9}$$

$$-\rho\left(\overline{u_\iota' u_k'}\frac{\partial \overline{U_J}}{\partial x_k} + \overline{u_\iota' u_k'}\frac{\partial \overline{U_\iota}}{\partial x_k}\right) - 2\mu\frac{\partial \overline{u_\iota}}{\partial x_k}\frac{\partial \overline{u_J}}{\partial x_k} - 2\rho\Omega_k(\overline{u_J' u_m'}\varepsilon_{ikm} + \overline{u_\iota' u_m'}\varepsilon_{jkm}) \tag{10}$$

$$\mu_t = \rho C_\mu \frac{k^2}{\varepsilon} \tag{11}$$

The constants in the above equations, $C_\mu = 0.09$, μ_t was the turbulent viscosity, the turbulence kinetic energy k and turbulence dissipation rate ε can be computed using the following Equations:

$$k = \frac{1}{2}\overline{u_i' u_j'} \tag{12}$$

$$\frac{\partial(\rho\varepsilon)}{\partial t} + \frac{(\partial \rho k \overline{U_j})}{\partial x_j} = -\frac{\partial}{\partial x_j}\left[\left(\mu + \frac{\mu_t}{\sigma_\varepsilon}\right)\frac{\partial \varepsilon}{\partial x_j}\right] + C_{\varepsilon 1}\rho\left(\overline{u_i' u_j'}\frac{\partial \overline{U_j}}{\partial x_k}\right)\frac{\varepsilon}{K} - C_{\varepsilon 2}\rho\frac{\varepsilon^2}{K} \tag{13}$$

where σ_ε=1.0, $C_{\varepsilon 1}$=1.44, and $C_{\varepsilon 2}$=1.92.

The mixing of the two liquid streams was simulated using the species transport equation, which can be expressed as:

$$\frac{\partial C_i}{\partial t} + U_j\frac{\partial C_i}{\partial x_j} = \frac{\partial}{\partial x_j}\left[(D + D_t)\frac{\partial C_i}{\partial x_j}\right] \tag{14}$$

The constant in Equation (14) was defined in the following values, C_i was the concentration of species i. D was the diffusion coefficient of the species, D_i was the turbulent diffusivity which was defined as:

$$D_t = \frac{\mu_t}{Sc_t} \tag{15}$$

The Schmidt number was denoted as Sc_t [43].

6-3. Boundary conditions

Water has been used as a solution A & B with a density of 98.2 kg/m^3 at 300 k, the flow rates of water A and water B were fixed as a ratio of 10, while the velocity of the water at the inlet A was set to depend on the diameter of the inlet. 5% of turbulent intensity at inlets A & B. A SIMPLE algorithm was applied. Furthermore, the simulation was considered to have reached the convergence criterion when the residuals of all governing equations' values dropped below 10^{-5}. A three-dimensional grid was made utilizing ANSYS ICEM-CFD. Grids having an alternate number of cells were trying to discover network-independent results, and a mesh containing 1.2 million computational cells was at the end. The Reynolds stress model has been demonstrated to be appropriate for computations within the RBR [15,106].

6-2. Evaluation of macromixing

Macromixing quality could be measured by the intensity of segregation (I_s) which depends on the concentration of species A & B, and was defined in Equation (1) [15].

The simulation results obtained by Xu-Jia Yue proved that the segregation intensity gradually decreased along the axial direction of the reactor, further indicating that the mixing condition gradually improved along the axial direction. The values of I_s increased with the decrease of the flow rate and rotational speed. This further showed that increasing the rotation speed and increasing the liquid flow rate can promote mixing between fluids both at the macroscopic level [108].

7. Conclusions

The specific measuring of macromixing within the Rotating bar reactor is of particular importance, as it will allow for the improvement of different process production and analyses. In the presented review, the fundamentals of assessing macromixing in an RBR through the intensity of the segregation system were illustrated. Over the years, experimental and simulation methods have been devised to measure macromixing. In this regard, the selection of measurement methods to study macromixing inside an RBR depends on the particulars of the process. The considerations encompass a blend of experimental goals, expenses related to equipment, postprocessing prerequisites, desired precision, and characteristics of the mixing reactor. Nevertheless, experimental techniques such as Conductivity, PLIF, and ERT have been studied. The important parameters were explained, such as materials used, equipment, procedures, experiment steps, and equations for I_s evaluation. Notably, the Conductivity technique was considered to be the simplest. In addition to applying CFD simulation of RBR to evaluate concentration distribution, then calculate the intensity of segregation. The incorporation of CFD methods in RBR required selecting rheological, turbulence, multiphase flow models, and boundary conditions. This paper gives a complete view of the fundamentals of how to use conductivity, PLIF, ERT, and CFD methods for measuring the intensity of segregation within RBR.

Acknowledgment

This work was supported by the Research Center of Sudan for High Gravity Chemical Engineering and Technology, Khartoum, Sudan.

Nomenclature

A : DI water
B : NaCl Solution
V_A : Volumetric flow rate of solution A, L/h (1 L/h=16.68 mL/min)
V_B : Volumetric flow rate of solution B, L/h
V : Total volumetric flow rate ($V_A + V_B$), L/h
d : Gap size of the RBR, mm
L : Length of the RBR, mm
I_s : Intensity of segregation
s_0 : Standard deviation
x_i : Mass fraction of a species at a certain grid point i
N : Rotational speed, rpm (1 rpm = 1 r/min)
C_{av} : The average concentration of NaCl solution, g/L (1 g/L=1 Kg/m^3)
C_{NaCl} : The concentration of NaCl solution at the feed inlet, g/L
$\bar{x}_{av}$: The average mass fraction

Dimensionless number

Re : Reynolds number, $Re = \rho\omega R_i d/\mu$

Γ : Aspect ratio, $\Gamma = L/d$

Abbreviations

RBR : Rotating Bar Reactor
TC : Taylor Couette
PLIF : Planar Laser Induced Fluorescence
CFD : Computational Fluid Dynamics
C_0V : The Coefficient of Variation
RTD : Residence Time Distribution
ERT : Electrical Resistance Tomography

References

1. Schrimpf, M., Esteban, J., Warmeling, H., Färber, T., Behr, A. and Vorholt, A. J., "Taylor-Couette Reactor: Principles, Design, and Applications," *AIChE J.*, **67**(5), 1-24(2021).
2. Banaga, A. B., Yue, X. J., Chu, G. W., Wu, W., Luo, Y. and Chen, J. F., "Micromixing Performance in a Rotating Bar Reactor," *Can. J. Chem. Eng.*, **98**(8), 1776-83(2020).
3. Gao, H. L., Wen, Z. N., Sun, B. C., Zou, H. K. and Chu, G. W., "Intensification of Ozone Mass Transfer for Wastewater Treatment Using a Rotating Bar Reactor," *Chem. Eng. Process. Process. Intensif.*, 176(2022).
4. Liu, Z. H., Wang, X. T., Liu, W., Gao, H. L. and Chu, G. W., "Mass Transfer Enhancement in a Rotating Bar Reactor: Gas Dispersion and Liquid Disturbance," *Chem. Eng. Process. Process. Intensif.*, **172**, 108774(2021).
5. Banaga, A. B., Li, Y. Bin, Li, Z. H., Sun, B. C. and Chu, G. W., "Experimental Investigation of the Mixing Efficiency via Intensity of Segregation along Axial Direction of a Rotating Bar Reactor," *Can. J. Chem. Eng.*, **59**, 153-59(2023).
6. Zhao, H., Shao, L. and Chen, J. F., "High-Gravity Process Intensification Technology and Application," *Chem. Eng. J.*, **156**(3), 588-93(2010).
7. Masuda, H., Yoshida, S., Horie, T., Ohmura, N. and Shimoyamada, M., "Flow Dynamics in Taylor–Couette Flow Reactor with Axial Distribution of Temperature," *AIChE. J.*, **64**(3), 1075-82(2018).
8. Dusting, J. and Balabani, S., "Mixing in a Taylor-Couette Reactor in the Non-Wavy Flow Regime," *Chem. Eng. Sci.*, **64**(13), 3103-3111(2009).
9. Nemri, M., Charton, S. and Climent, E., "Mixing and Axial Dispersion in Taylor-Couette Flows: The Effect of the Flow Regime," *Chem. Eng. Sci.*, **139**, 109-24(2015).
10. Bin, L., Guang, L., Xiaogang, Y., Shanshan, L., Yingrong, X., Lu, L., and Yuan, Z., "Micro-mixing enhancement in a Taylor-Couette Reactor Using the Inner Rotors with Various Surface Configurations," *Chem. Eng. Process. Process. Intensif.*, **204**, 109954(2024).
11. Mao, Z. and Yang, C., "Micro-Mixing in Chemical Reactors: A Perspective," *Chinese. J. Chem. Eng.*, **25**(4), 381-90(2016).
12. Woldemariam, M., Filimonov, R., Purtonen, T., Sorvari, J., Koiranen, T. and Eskelinen, H., "Mixing Performance Evaluation of Additive Manufactured Milli-Scale Reactors," *Chem. Eng. Sci.*, **152**, 26-34(2016).
13. Wenzel, D. and Górak, A., "Review and Analysis of Micromixing in Rotating Packed Beds," *Chem. Eng. J.*, **345**, 492-506(2018).
14. Jaworski, Z. and Dudczak, J., "CFD Modelling of Turbulent Macromixing in Stirred Tanks. Effect of the Probe Size and Number on Mixing Indices," *Comp. Chem. Eng.*, **22**(1), S293-S298(1998).
15. Luo, J. Z., Luo, Y., Chu, G. W., Arowo, M., Xiang, Y., Sun, B. C. and Chen, J. F., "Micromixing Efficiency of a Novel Helical Tube Reactor: CFD Prediction and Experimental Characterization," *Chem. Eng. Sci.*, 155, 386-396(2016).
16. Yang, K., Chu, G. W., Shao, L., Luo, Y. and Chen, J. F., "Micromixing Efficiency of Rotating Packed Bed with Premixed Liquid Distributor," *Chem. Eng. J.*, **153**(1-3), 222-226(2009).
17. Baldyga, J., Bourne, J. R. and Yang, Y., "Influence of Feed Pipe Diameter on Mesomixing in Stirred Tank Reactors," *Chem. Eng. Sci.*, **48**(19), 3383-3390(1993).
18. Villermaux, J. and Falk, L., "A Generalized Mixing Model for Initial Contacting of Reactive Fluids," *Chem. Eng. Sci.*, **49**(24), 5127-5140(1994).
19. Barresi, A. A., Marchisio, D. and Baldi, G., "On the Role of Micro- and Mesomixing in a Continuous Couette-Type Precipitator," *Chem. Eng. Sci.*, **54**(13-14), 2339-2349(1999).
20. Barrett, M., O'Grady, D., Casey, E. and Glennon, B., "The Role of Meso-Mixing in Anti-Solvent Crystallization Processes," *Chem. Eng. Sci.*, **66**(12), 2523-2534(2011).
21. Baldyga, J. and Bourne, J. R., "A Fluid Mechanical Approach to Turbulent Mixing and Chemical Reaction Part II Micromixing in the Light of Turbulence Theory," *Chem. Eng. Commun.*, **28**(4-6), 243-258(1984).
22. Tsai, B. I., Erickson, L. E. and Fan, L. T., "The Effect of Micromixing on Growth Processes," *Biotechnol. Bioeng.*, **11**(2), 181-205(1969).
23. Nie, A., Gao, Z., Xue, L., Cai, Z., Evans, G. M. and Eaglesham, A., "Micromixing Performance and the Modeling of a Confined Impinging Jet Reactor/High Speed Disperser," *Chem. Eng. Sci.*, **184**, 14-24(2018).
24. Kling, K. and Mewes, D., "Two-Colour Laser Induced Fluorescence for the Quantification of Micro- and Macromixing in Stirred Vessels," *Chem. Eng. Sci.*, **59**(7), 1523-1528(2004).
25. Kukukova, A., Aubin, J. and Kresta, S. M., "A New Definition of Mixing and Segregation: Three Dimensions of a Key Process Variable," *Chem. Eng. Res. Des.*, **2009**, 87(4), 633-47(2009).
26. Danckwerts, P. V., "The Definition and Measurement of Some Characteristics of Mixtures," *Appl. Sci. Res. Sect. A.*, **3**(4), 279-96 (1952).
27. Bakker, R. A. and Akker, H. E. A., "Van Den, A Lagrangian Description of Micromixing in a Stirred Tank Reactor Using 1D-Micromixing Models in a CFD Flow Field," *Chem. Eng. Sci.*, **51**(11), 2643-2648(1996).
28. Pagnini, G., "The Kernel Method to Compute the Intensity of Segregation for Reactive Pollutants: Mathematical Formulation," *Atmos. Environ.*, **43**(24), 3691-3698(2009).
29. Buchmann, M. and Mewes, D., "Tomographic Measurements of Micro- and Macromixing Using the Dual Wavelength Photometry," *Chem. Eng. J.*, **77**(1-2), 3-9(2000).
30. Luo, P., Jia, H., Xin, C., Xiang, G., Jiao, Z. and Wu, H., "An Experimental Study of Liquid Mixing in a Multi-orifice-impinging Transverse Jet Mixer Using PLIF," *Chem. Eng. J.*, **228**, 554-564(2013).

31. Tahvildarian, P., Ng, H., D'Amato, M., Drappel, S., Ein-Mozaffari, F. and Upreti, S. R., "Using Electrical Resistance Tomography Images to Characterize the Mixing of Micron-Sized Polymeric Particles in a Slurry Reactor," *Chem. Eng. J.*, **172**(1), 517-525(2011).
32. Battaglia, G., Romano, S., Raponi, A., Volpe, F., Bellanca, L., Ciofalo, M., Marchisio, D., Cipollina, A., Micale, G. and Tamburini, A., "Mixing Phenomena in Circular and Rectangular Cross-Sectional T-Mixers: Experimental and Numerical Assessment," *Chem. Eng. Res. Des.*, **201**, 228-241(2023).
33. Arratia, P. E. and Muzzio, F. J., "Planar Laser-Induced Fluorescence Method for Analysis of Mixing in Laminar Flows," *Ind. Eng. Chem. Res*., **43**(20), 6557-6568(2004).
34. Taghavi, M. and Moghaddas, J., "Using PLIF/PIV Techniques to Investigate the Reactive Mixing in Stirred Tank Reactors with Rushton and Pitched Blade Turbines," *Chem. Eng. Res. Des*., **151**, 190-206(2019).
35. Mosorov, V., "Applications of Tomography in Reaction Engineering (Mixing Process)," *Ind. Tomogr. Syst. Appl.*, 509-228(2015).
36. Bowler, A. L., Bakalis, S. and Watson, N. J., "A Review of In-Line and on-Line Measurement Techniques to Monitor Industrial Mixing Processes," *Chem. Eng. Res. Des*., **153**, 463-495(2019).
37. Haddadi, M. M., Hosseini, S. H., Rashtchian, D. and Olazar, M., "Comparative Analysis of Different Static Mixers Performance by CFD Technique: An Innovative Mixer," *Chinese J. Chem. Eng.*, **28**(3), 672-684(2019).
38. Zhang, Y.-D., Zhang, C.-L., Zhang, L.-L., Sun, B.-C., Chu, G.-W. and Chen, J.-F., "Chemical Probe Systems for Assessing Liquid–Liquid Mixing Efficiencies of Reactorse," *Front. Chem. Sci. Eng.*, **17**(10), 1323-1335(2023).
39. Martínez-Delgadillo, S. A., Mollinedo P., H. R., Gutiérrez, M. A., Barceló, I. D. and Méndez, J. M., "Performance of a Tubular Electrochemical Reactor, Operated with Different Inlets, to Remove Cr(VI) from Wastewater," *Comput. Chem. Eng.*, **34**(4), 491-499(2009).
40. Wilkinson, N. A. and Dutcher, C. S., "Axial Mixing and Vortex Stability to in Situ Radial Injection in Taylor-Couette Laminar and Turbulent Flows," *J. Fluid. Mech.*, **854**, 324-347(2018).
41. Judat, B., Racina, A. and Kind, M., "Macro- and Micromixing in a Taylor-Couette Reactor with Axial Flow and Their Influence on the Precipitation of Barium Sulfate," *Chem. Eng. Tech.*, **27**(3), 287-292(2004).
42. Banaga, A. B., "Mixing in a Rotating Bar Reactor and Application in Wastewater Treatment". Ph.D. Thesis, Beijing University of Chemical Technology, Beijing(2023).
43. Li, G., Yang, X. and Ye, H., "CFD Simulation of Shear Flow and Mixing in a Taylor-Couette Reactor with Variable Cross-Section Inner Cylinders," *Pow. Tech.*, **280**, 53-66(2015).
44. Habchi, C., Valle, D. Della, Lemenand, T., Anxionnaz, Z., Tochon, P., Cabassud, M., Gourdon, C. and Peerhossaini, H., "A New Adaptive Procedure for Using Chemical Probes to Characterize Mixing," *Chem. Eng. Sci.*, **66**(15), 3540-3550(2011).
45. Patrizio, N. Di, Bagnaro, M., Gaunand, A., Hochepied, J. F., Horbez, D. and Pitiot, P., "Hydrodynamics and Mixing Performance of Hartridge Roughton Mixers: Influence of the Mixing Chamber Design," *Chem. Eng. J*., **283**, 375-387(2015).
46. Bałdyga, J., Henczka, M. and Makowski, "Effects of Mixing on Parallel Chemical Reactions in a Continuous-Flow Stirred-Tank Reactor," *Chem. Eng. Res. Des.*, **79**(8), 895-900(2001).
47. Hjertager, L. K., Hjertager, B. H., Deen, N. G. and Solberg, T., "Measurement of Turbulent Mixing in a Confined Wake Flow Using Combined PIV and PLIF," *Can. J. Chem. Eng*., **81**(6), 1149-1158(2003).
48. Alena, K., Benjamin N.l., and Suzanne M. K., "Impact of Sampling Method and Scale on the Measurement of Mixing and the Coefficient of Variance," *AIChE. J*., **54**(12), pp. 3068-3083(2008).
49. Cheng, D., Feng, X., Cheng, J., Yang, C. and Mao, Z. S., "Experimental Study on the Dispersed Phase Macro-Mixing in an Immiscible Liquid-Liquid Stirred Reactor," *Chem. Eng. Sci.*, **126**, 196-203(2014).
50. Paul, E. L., Atiemo-obeng, V. A. and Kresta, S. M., Handbook of Industrial Mixing Edited By, Handbook of Industrial Mixing Science and Practice, (2015).
51. Lehwald, A., Thévenin, D. and Zähringer, K., "Quantifying Macro-Mixing and Micro-Mixing in a Static Mixer Using Two-Tracer Laser-Induced Fluorescence," *Exp. Fluids*., **48**(5), 823-836(2010).
52. Houcine, I., Vivier, H., Plasari, E., David, R. and Villermaux, J., "Planar Laser Induced Fluorescence Technique for Measurements of Concentration Fields in Continuous Stirred Tank Reactors," *Exp. Fluids*., **22**(2), 95-102(1996).
53. Shen, B., Zhan, X., Sun, Z., He, Y., Long, J. and Li, X., "PIV Experiments and CFD Simulations of Liquid–Liquid Mixing in a Planetary Centrifugal Mixer (PCM)," *Chem. Eng. Sci.*, **259**, 117764(2022).
54. Prończuk, M. and Bizon, K., "Investigation of the Liquid Mixing Characteristic of an External-Loop Hybrid Fluidized-Bed Airlift Reactor," *Chem. Eng. Sci*., **210**, 115231(2019).
55. Li, X., Mi, Z., Tan, S., Wang, X., Wang, R. and Ding, H., "Experimental Investigation of Fluid Mixing inside a Rod Bundle Using Laser Induced Fluorescence," *Prog. Nucl. Energy*., **110**, 90-102 (2018).
56. Wang, X., Wang, R., Du, S., Chen, J. and Tan, S., "Flow Visualization and Mixing Quantification in a Rod Bundle Using Laser Induced Fluorescence," *Nucl. Eng. Des*., **305**, 1-8(2016).
57. Gaskey, S., Vacus, P., David, R., Villermaux, J. and André, J. C., "A Method for the Study of Turbulent Mixing Using Fluorescence Spectroscopy," *Exp. Fluids*., **9**(3), 137-147(1990).
58. Lozano, A., Yip, B. and Hanson, R. K., "Acetone: A Tracer for Concentration Measurements in Gaseous Flows by Planar Laser-Induced Fluorescence," *Exp. Fluids*., **13**(6), 369-376(1992).
59. Li, C., Wu, B., Zhang, J. and Luo, P., "Effect of Swirling Addition on the Liquid Mixing Performance in a T-Jets Mixer," *Chines. J. Chem. Eng.*, **50**, 108-116(2022).
60. Eltayeb, A., Tan, S., Qi, Z., Ala, A. A. and Ahmed, N. M., "PLIF Experimental Validation of a FLUENT CFD Model of a Coolant Mixing in Reactor Vessel Down-Comer," *Annals of Nucl. Energ*., **128**, 190-202(2018).
61. Bedding, D. C. and Hidrovo, C. H., "Dual Fluorescence Ratiometric Technique for Micromixing Characterization," *Exp. Fluids.*, **59**(11), (1018).
62. Carroll, B. and Hidrovo, C., "Droplet Collision Mixing Diagnostics Using Single Fluorophore LIF," *Exp. Fluids*., **53**(5), 130-1316 (2012).
63. Ascanio, G., "Mixing Time in Stirred Vessels: A Review of Experimental Techniques," *Chines. J. Chem. Eng*., **23**(7), 1065-

1076(2014).
64. Luo, P., Cheng, Y., Wang, Z., Jin, Y. and Yang, W., "Study on the Mixing Behavior of Thin Liquid-Sheet Impinging Jets Using the PLIF Technique," *Ind. Eng. Chem. Res*., **45**(2), 863-870(2006).
65. Jardón-Pérez, L. E., González-Rivera, C., Trápaga-Martínez, G., Amaro-Villeda, A. and Ramírez-Argáez, M. A., "Experimental Study of Mass Transfer Mechanisms for Solute Mixing in a Gas-Stirred Ladle Using the Particle Image Velocimetry and Planar Laser-Induced Fluorescence Techniques," *Steel. Res. Int*., **92**(11), 1-11(2021).
66. Moulijn, J., The Chemicfll Processing Pmnt, World Wide Web Internet And Web Information Systems, (2004).
67. Rida, Z., Cazin, S., Lamadie, F., Dherbécourt, D., Charton, S., and Climent, E., "Experimental Investigation of Mixing Efficiency in Particle-Laden Taylor–Couette Flows," *Exp. Fluids*., **60**(61), (2019).
68. Walker, D. A., "A Fluorescence Technique for Measurement of Concentration in Mixing Liquids," *J. Physics. E: Scient. Inst*., **20**(2), 217-224(1987).
69. Coppeta, J. and Rogers, C., "Dual Emission Laser Induced Fluorescence for Direct Planar Scalar Behavior Measurements," *Exp. Fluids*., **25**(1), 1-15(1998).
70. Saylor, J. R., "Photobleaching of Disodium Fluorescein in Water," *Exp. Fluids.*, **18**(6), 445-447(1995).
71. Crimaldi, J. P., "The Effect of Photobleaching and Velocity Fluctuations on Single-Point LIF Measurements," *Exp. Fluids*., **23**(4), 325-330(1997).
72. Larsen, L. G. and Crimaldi, J. P., "The Effect of Photobleaching on PLIF," *Exp. Fluids*., **41**(5), 803-812(2006).
73. Unger, D. R. and Muzzio, F. J., "Laser-Induced Fluorescence Technique for the Quantification of Mixing in Impinging Jets," *AIChE. J*., **45**(12), 2477-2486(1999).
74. Bruchhausen, M., Guillard, F. and Lemoine, F., "Instantaneous Measurement of Two-Dimensional Temperature Distributions by Means of Two-Color Planar Laser Induced Fluorescence (PLIF)," *Exp. Fluids*., **38**(1), 123-131(2005).
75. Lemoine, F., Antoine, Y., Wolff, M. and Lebouche, M., "Simultaneous Temperature and 2D Velocity Measurements in a Turbulent Heated Jet Using Combined Laser-Induced Fluorescence and LDA," *Exp. Fluids*., **26**(4), 315-323(1999).
76. Laidlaw, I. M. S. and Smart, P. L., "An Evaluation of Some Fluorescent Dyes for Water Tracing," *Water. Res. Res*., **13**(1), 15-33 (1977).
77. Fonte, S. M. W. B. P. M. A. K. C. P., "Investigation of Mixing Miscible Liquids with High Viscosity Contrasts in Turbulently Stirred Vessels Using Electrical Resistance Tomography," *Chem. Eng. J*., **486**, 149712(2024).
78. Sharifi, M. and Young, B., "Electrical Resistance Tomography (Ert) Applications to Chemical Engineering," *Chem. Eng. Res. Des*., **91**(9), 1625-1645(2013).
79. Stephenson, D. R., Cooke, M., Kowalski, A. and York, T. A., "Determining Jet Mixing Characteristics Using Electrical Resistance Tomography," *Flow Meas. Instrum*., **18**(5-6), 204-210(2007).
80. Jegatheeswaran, S. and Ein-Mozaffari, F., "Investigation of the Detrimental Effect of the Rotational Speed on Gas Holdup in Non-Newtonian Fluids with Scaba-Anchor Coaxial Mixer: A Paradigm Shift in Gas-Liquid Mixing," *Chem. Eng. J*., **383**, 123118(2019).
81. Kazemzadeh, A., Ein-Mozaffari, F. and Lohi, A., "Mixing of Highly Concentrated Slurries of Large Particles: Applications of Electrical Resistance Tomography (ERT) and Response Surface Methodology (RSM)," *Chem. Eng. Res. Des*., **143**, 226-240(2019).
82. Park, B. G., Moon, J. H., Lee, B. S. and Kim, S., "An Electrical Resistance Tomography Technique for the Monitoring of a Radioactive Waste Separation Process," *Int. Commun. Heat. Mass. Transf*., **35**(10), 1307-1310(2008).
83. Jin, H., Wang, M. and Williams, R. A., "Analysis of Bubble Behaviors in Bubble Columns Using Electrical Resistance Tomography," *Chem. Eng. J*., **130**(2-3), 179-185(2007).
84. Bolton, G. T., Hooper, C. W., Mann, R. and Stitt, E. H., "Flow Distribution and Velocity Measurement in a Radial Flow Fixed Bed Reactor Using Electrical Resistance Tomography," *Chem. Eng. Sci*., **59**(10), 1989-1997(2004).
85. Bond, J., Cullivan, J. C., Climpson, N., Dyakowski, T., Faulks, I., Jia, X., Kostuch, J. A., Payton, D., "Industrial Monitoring of Hydrocyclone Operation Using Electrical Resistance Tomography," *1st World Congr. Ind. Process Tomogr*, **12**(10), 102-107(1999).
86. Zbib, H., Ebrahimi, M., Ein-Mozaffari, F. and Lohi, A., "Hydrodynamic Behavior of a 3-D Liquid-Solid Fluidized Bed Operating in the Intermediate Flow Regime - Application of Stability Analysis, Coupled CFD-DEM, and Tomography," *Ind. Eng. Chem. Res*., **57**(49), 16944-16957(2018).
87. Mann, R., Dickin, F. J., Wang, M., Dyakowski, T., Williams, R. A., Edwards, R. B., Forrest, A. E. and Holden, P. J., "Application of Electrical Resistance Tomography to Interrogate Mixing Processes at Plant Scale," *Chem. Eng. Sci.*, **52**(13), 2087-2097(1997).
88. Stanley, S. J. and Bolton, G. T., "A Review of Recent Electrical Resistance Tomography (ERT) Applications for Wet Particulate Processing," *Part. Part. Syst. Charact*., **25**(3), 207-215(2008).
89. Špidla, M., Sinevič, V., Jahoda, M. and MacHoň, V., "Solid Particle Distribution of Moderately Concentrated Suspensions in a Pilot Plant Stirred Vessel," *Chem. Eng. J.*, **113**(1), 73-82(2005).
90. Yenjaichon, W., Pageau, G., Bhole, M., Bennington, C. P. J. and Grace, J. R., "Assessment of Mixing Quality for an Industrial Pulp Mixer Using Electrical Resistance Tomography," *Can. J. Chem. Eng*., **89**(5), 996-1004(2011).
91. Pakzad, L., Ein-Mozaffari, F. and Chan, P., "Measuring Mixing Time in the Agitation of Non-Newtonian Fluids through Electrical Resistance Tomography," *Chem. Eng. Tech*., **31**(12), 1838-1845(2008).
92. Hosseini, S., Patel, D., Ein-Mozaffari, F. and Mehrvar, M., "Study of Solid-Liquid Mixing in Agitated Tanks through Electrical Resistance Tomography," *Chem. Eng. Sci.*, **65**(4), 1374-1384(2009).
93. Carletti, C., Montante, G., Westerlund, T. and Paglianti, A., "Analysis of Solid Concentration Distribution in Dense Solid-Liquid Stirred Tanks by Electrical Resistance Tomography," *Chem. Eng. Sci*., **119**, 53-64(2014).
94. Mirshekari, F. and Pakzad, L., "Mixing of Oil in Water Through Electrical Resistance Tomography and Response Surface Methodology," *Chem. Eng. Tech*., **42**(5), 1101-1115(2019).
95. Maluta, F., Montante, G. and Paglianti, A., "Analysis of Immiscible Liquid-Liquid Mixing in Stirred Tanks by Electrical Resistance Tomography," *Chem. Eng. Sci*., **227**, 115898(2020).
96. Yao, Z., Alberini, F., Montante, G. and Paglianti, A., "In-Line Monitoring of Mixing Performance for Smart Processes in Tubular Reactors," *Chem. Eng. Res. Des*., **194**, 678-692(2023).

97. Qureshi, M. F., Ali, M. H., Ferroudji, H., Rasul, G., Khan, M. S., Rahman, M. A., Hasan, R. and Hassan, I., "Measuring Solid Cuttings Transport in Newtonian Fluid across Horizontal Annulus Using Electrical Resistance Tomography (ERT)," *Flow Meas. Instrum.*, **77**, 101841(2020).
98. Alberini, F., Simmons, M. J. H., Ingram, A. and Stitt, E. H., "Assessment of Different Methods of Analysis to Characterise the Mixing of Shear-Thinning Fluids in a Kenics KM Static Mixer Using PLIF," *Chem. Eng. Sci*., **112**, 152-169(2014).
99. Li, L., Wang, K., Zhao, Q., Gao, Q., Zhou, H., Jiang, J. and Mei, W., "A Critical Review of Experimental and CFD Techniques to Characterize the Mixing Performance of Anaerobic Digesters for Biogas Production," *Rev. Environ. Sci. Biotechnol.*, **21**(3), 665-689(2022).
100. Forte, G., Albano, A., Simmons, M. J. H., Stitt, H. E., Brunazzi, E. and Alberini, F., "Assessing Blending of Non-Newtonian Fluids in Static Mixers by Planar Laser-Induced Fluorescence and Electrical Resistance Tomography," *Chem. Eng. Tech.*, **42**(8), 1602-1610(2019).
101. Parvizian, F., Rahimi, M. and Azimi, N., "Macro- and Micromixing Studies on a High Frequency Continuous Tubular Sonoreactor," *Chem. Eng. Process. Process Intensif.*, **57-58**, 8-15(2012).
102. Mohammadi, S. and Boodhoo, K. V. K., "Online Conductivity Measurement of Residence Time Distribution of Thin Film Flow in the Spinning Disc Reactor," *Chem. Eng. J.*, **207-208**, 885-894 (2012).
103. Zheng, H., Huang, Z., Liao, Z., Wang, J., Yang, Y. and Wang, Y., "Computational Fluid Dynamics Simulations and Experimental Validation of Macromixing and Flow Characteristics in Low-Density Polyethylene Autoclave Reactors," *Ind. Eng. Chem. Res*., **53**(38), 14865-14875(2014).
104. Xu, X., Zhang, J., Chen, J., Zhao, D., Zhang, J. and Qin, S., "Numerical Investigation of Mixing Performance for a Helical Tangential Porous Tube-in-Tube Microchannel Reactor," *Chem. Eng. Process. Process Intensif*., **200**, 109766(2024).
105. Liu, L., Yang, X., Yang, J., Li, G. and Guo, Y., "Effect of Hydrodynamic Heterogeneity on Micromixing Intensification in a Taylor–Couette Flow Reactor with Variable Configurations of Inner Cylinder," *AIChE. J*., **67**(7), 1-13(2021).
106. Liu, F., Yang, X. and Wang, R., "Micromixing Performance in a Taylor–Couette Reactor with Ribbed Rotors," *Process. Artic*., **11**, 2058(2023).
107. Vedantam, S., Joshi, J. B. and Koganti, S. B., "CFD Simulation of RTD and Mixing in the Annular Region of a Taylor-Couette Contactor," *Ind. Eng. Chem. Res.*, **45**(18), 6360-6367(2006).
108. Yue, X.-J., "Flow and Mixing Characteritics of Rotating Bar Reactor," Ms.c. Thesis: Beijing University of Chemical Technology, Beijing(2019).

Authors

Abdelgadir Bashir Banaga: Ph. D., Principal researcher, Department of Transportation & Refining Engineering, College of Petroleum Engineering & Technology, Sudan University of Science & Technology, Sudan; asad.85@hotmail.com

Zeinab A. M. Khalel: Ph. D., Researcher, Department of Transportation & Refining Engineering, College of Petroleum Engineering & Technology, Sudan University of Science & Technology; zeinabkhaleel@yahoo.com